Mechanical characterisation of miniaturised direct inkjet printed 3Y-TZP specimens for microelectronic applications

Emre Özkol [a],*, Anja M. Wätjen [a], Raúl Bermejo [b], Marco Deluca [b,c], Jörg Ebert [a], Robert Danzer [b,c], Rainer Telle [a]

[a] *Department of Ceramics and Refractory Materials, RWTH Aachen University, Mauerstraße 5, D-52064 Aachen, Germany*
[b] *Institut für Struktur- und Funktionskeramik (ISFK), Montanuniversität Leoben, Peter-Tunner Straße 5, A-8700 Leoben, Austria*
[c] *Materials Center Leoben Forschung GmbH, Roseggerstraße 12, A-8700 Leoben, Austria*

Abstract

Direct inkjet printing (DIP) allows the production of small ceramic specimens with special geometries starting from high solids content suspensions. In this work, thin (300 μm thickness) 3Y-TZP specimens were produced with the DIP technique as model materials for microelectronic applications. The mechanical strength of the printed specimens was evaluated under biaxial loading, and the results were interpreted within the framework of the Weibull theory. Hot-pressed 3Y-TZP specimens with the same geometry and dimensions were tested for comparison. The fracture surfaces were subsequently examined using scanning electron microscopy (SEM). The inkjet printed materials revealed high mechanical reliability ($m \approx 10$ for $\sigma_0 \approx 1400$ MPa), which was ascribed to the uniform and defect free microstructure generated by the DIP technique.
© 2010 Elsevier Ltd. All rights reserved.

Keywords: Platelets; Mechanical properties; Strength; ZrO$_2$; Direct inkjet printing

1. Introduction

Direct inkjet printing (DIP) is a typical solid freeform fabrication (SFF) method, which includes the following general steps: (a) the design and generation of a three-dimensional computer model, (b) the conversion of the model into two-dimensional data, and (c) the fabrication of the three-dimensional object. In the DIP process the fabrication is realised by the selective deposition of identical drops of a particulate suspension using an ink deposition nozzle. The DIP method became popular for ceramic materials in the 1990s and several studies have demonstrated the feasibility of inkjet printing in this material field.[1–5] However, these pioneering studies were not successful in fabricating accurately shaped three-dimensional objects, mostly because of drying difficulties of low solids content inks. In order to overcome this, two different approaches were developed in the 2000s. The first approach was to develop phase-change inks which rapidly solidify upon rapid cooling,[6–9] yielding a relatively high printing rate. However, the surface of each printed layer must be flattened before the next layer is deposited in order to ensure the shape accuracy. Another disadvantage is the low green density and high wax content of the printed objects, which makes a complicated wax removal step necessary prior to the sintering step. The second approach was to assist the drying of the deposited ink externally, when aqueous or solvent based inks were printed.[10–14] In this case the position of the deposited layers is fixed due to the accelerated drying, which provides good shape accuracy with sharp edges and corners. Such accuracy depends on the ink composition and the drying intensity as well as the surface/volume ratio of the printed objects.

Precise structures such as micro pillars or micro walls have been produced by DIP without any drying assistance.[15–17] However, in case of producing relatively large (mm to cm scale) objects, the drying must be controlled. Moreover, the drying conditions must be optimised for every ink composition and object geometry in order to provide shape accuracy and avoid distortion due to drying stresses, which may lead to delamination. In this regard drying-assisted printed objects show a higher green density compared to objects printed using phase-change inks. The achievement of high green density is a prerequisite to

* Corresponding author. Tel.: +49 2418094981; fax: +49 2418092226.
E-mail address: oezkol@ghi.rwth-aachen.de (E. Özkol).

produce ceramic components with good mechanical properties, as it has been recently demonstrated by some of the authors.[13,14]

In this work the DIP process has been used as a means to produce small ceramic specimens to be used in microelectronics (*e.g.* printed circuit boards – PCB[18,19]). 3 mol% yttria stabilised tetragonal zirconia (3Y-TZP) specimens were fabricated in two different geometries (2 mm × 2 mm and 3 mm × 4 mm), both with a thickness of ≈300 μm. The use of small ceramic specimens in the microelectronics industry is a growing trend motivated by miniaturisation, which can be achieved by reducing the size of electronic circuits and/or embedding the components. Consequently, small ceramic specimens such as capacitors, transformers, *etc.* not only have to match the size requirements of the circuit producers, but must also be able to withstand the severe biaxial stresses which may arise for instance during thermal pressing processes (common for PCB). Therefore, testing the mechanical properties of small ceramic specimens prior to their use as electronic components has become a mandatory yet complicated task for the vast majority of producers.

Brittle ceramic materials usually fail according to a defect distribution, for which the weakest-link-hypothesis is valid: the failure of a specimen is triggered by the largest flaw contained in its volume. For most brittle materials, the size frequency density of defects decreases with increasing crack size, and in this case Weibull statistics can be employed to describe the probability of failure, *F*, of a given specimen as[20,21]:

$$F(\sigma, V) = 1 - \exp\left[1 - \frac{V}{V_0}\left(\frac{\sigma}{\sigma_0}\right)^m\right], \qquad (1)$$

where σ is the applied stress, and V the specimen volume. The Weibull modulus m describes the scatter of the strength distribution. The characteristic strength σ_0 is the stress at which the failure probability is ≈63%, if $V = V_0$, where V_0 is the reference volume.

The Weibull theory[20,21] has proven to be very effective in describing the behaviour of this class of materials; however, it has been proposed[22] that modifications to the theory or more accurate investigations might be necessary in the case of small probes for microelectronics. As a general rule, in order to analyse the fracture statistics of a material it is a good practice to test specimens of different geometries with a well-controlled strength test. If an extrapolation for strength design purposes is not contemplated, the Weibull distribution can still be used to represent strength data also in very small specimens.[21]

According to the biaxial nature of the stresses that can develop during pressing of components into common electric circuits, it is necessary to assess the strength of the ceramic material by means of a biaxial fixture. In this work, the ball-on-three-balls (B3B) test[23–26] has been employed for the determination of the strength of the direct inkjet printed 3Y-TZP samples. This method has been recently renowned as one of the most effective testing procedures for thin brittle rectangular plates.[23–26] In fact, the well-defined load transfer to the specimen allows overcoming the geometric inaccuracies that could be involved in using ring-on-ring or ball-on-ring fixtures.[27,28] The test results have been evaluated within the framework of the Weibull theory

for small specimens, and compared with results of B3B tests on commercial hot-pressed 3Y-TZP specimens with the same geometry. In addition, the fracture surfaces of selected specimens after failure have been examined by means of SEM. A discussion on the differences in the strength behaviour of samples produced with both DIP and hot-pressing is provided in terms of the size and shape of critical defects.

2. Experimental procedure

2.1. Preparation of the ceramic ink

Sub-micron sized 3Y-TZP particles (TZ-3YS-E, Tosoh Inc., Japan) were dispersed in an aqueous medium using a commercial carboxylic acid-based dispersant (Dolapix CE64, Zschimmer&Schwarz, Germany). A suspension with 40 vol.% solids content and 0.5 wt.% (related to solids) dispersant was homogenised by attrition milling at 1200 rpm for 30 min. The particle size distribution of the milled suspension was determined by means of laser scattering (Mastersizer 2000, Malvern Instruments, UK).

Aqueous ceramic suspensions can be used for inkjet printing provided they include some specific additives, especially humectants.[29,30] In a previous study the influence of several organic humectants on the printability was investigated and a printable 3Y-TZP ink with 24 vol.% of solids and ∼20 vol.% of humectants was developed.[16] A following study showed that when three-dimensional objects are to be generated, besides printability, a proper drying of the deposited layers is also an important aspect.[17] In order to assist drying of layers the solids content of the previously developed ceramic ink was increased to 27 vol.%, while keeping the content of additives unchanged.

The ink was characterised at 20 °C in terms of viscosity and surface tension. The viscosity was determined at a shear rate of $1000\,s^{-1}$ using a rotational rheometer (Viscolab LC10, Physica, Germany) with a double gap concentric measuring system. The surface tension of the ink was determined according to the bubble pressure method (Proline t15, Sita Corp., Germany) for a bubble lifetime of 0.5 s.

The drop formation behaviour of the inkjet inks can be described by the physical properties of the ink. Previous studies summarised these properties using the inverse of the Ohnesorge number (Oh), and defined the region of printability as $1 < Oh^{-1} < 10$.[6,8,31] The Oh^{-1} number is defined by:

$$Oh^{-1} = \frac{(\sigma \cdot \rho \cdot a)^{1/2}}{\eta}, \qquad (2)$$

where σ is the surface tension of the ink, ρ is the density, a is a characteristic length (nozzle radius), and η is the viscosity. The Oh^{-1} number of the 3Y-TZP ink was calculated and compared to previously published results.

The drop formation and drop characteristics were also experimentally analysed. An array of single drops, which were printed on a glass object plate, was analysed with SEM (Leo 440 SEM, Leo, Germany). The printer settings and the detailed procedure of this experiment can be found elsewhere.[17]

2.2. Direct inkjet printing (DIP)

The ceramic ink was printed with an office-type thermal inkjet printer (HP Deskjet 930c®) using black ink cartridges (HP51645A). The integrated printing head presents 300 identical nozzles of 30 μm in diameter. Black cartridges were emptied, flushed thoroughly with water and placed in an ultrasonic cleaner until no traces of ink were visible. After cleaning, the cartridges were dried completely in order to avoid a possible dilution of the ceramic ink by remaining water. Subsequently, they were filled with 40 ml of ceramic ink and the residual air inside was evacuated.

The print orders were realised using the original driver of the printer and MS Word® documents containing the figures of the intended cross-sectional shapes. These figures were filled with black colour (RGB: 0/0/0) and the monochrome printing mode was selected in order to print the complete area. The over-printing needed to produce three-dimensional objects was provided by disabling the sensor controlling the presence of paper. The substrate was always placed on the printing path. In order to facilitate the drying of the printed layers the substrates were heated up to 80 °C prior to printing. A 300 W spotlight was used to keep the substrate temperature constant during printing.

Two groups of testing specimens were produced. The dimensions of the printed cross-sectional areas of the specimens were 2.35 mm × 2.35 mm and 3.5 mm × 4.7 mm. A graphite substrate (SGL Carbon, Germany) was used and all the specimens consisted of 65 layers deposited on top of each other.

All the samples were dried at room temperature and subsequently stored at 80 °C for 12 h. A 3 h heat treatment at 850 °C was applied to separate the printed 3Y-TZP samples from the substrate. Subsequently, the specimens were sintered for 2.5 h in a ZrO_2 powder bed at 1450 °C.

2.3. Mechanical testing

The mechanical strength of the inkjet printed 3Y-TZP specimens of study was determined under biaxial flexure using the ball-on-three-balls (B3B) test. For comparison two commercial 3Y-TZP samples prepared with a different method (Z900, Morgan Technical Ceramics, UK – hot-pressed at 140 MPa and 1450–1550 °C) were cut in the form of 2 mm × 2 mm and 3 mm × 4 mm platelets of ≈300 μm thickness, and tested under the same conditions. A schematic of the B3B testing apparatus is displayed in Fig. 1(a). The specimen is centrally positioned over the loading ball, and is supported by three balls on the upper surface. A circular guide ensures that all four balls and the specimen are carefully aligned. During testing a preload (typically about 10% of the estimated fracture load) is initially applied. After that, the positioning aid (chock) is pushed down and the supporting balls can freely move, while the loading ball is kept fixed. Friction forces keep the specimen and the balls firmly in this position. Subsequently, the load is increased until fracture occurs, and the fracture load can be used to calculate the maximum tensile biaxial stress in the specimen at the moment of
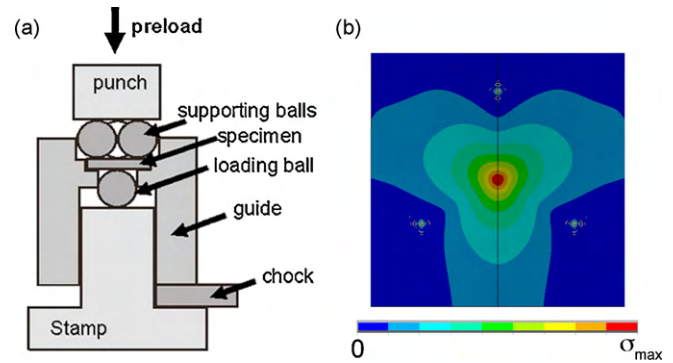

Fig. 1. (a) Schematic of the B3B fixture for biaxial testing of thin rectangular specimens. (b) FE simulation of the biaxial stress field in the tensile side of the specimen.

fracture, given by:

$$\sigma_{max} = f \frac{P}{t^2}, \tag{3}$$

where P is the maximum load at fracture, and t the specimen thickness. f is a dimensionless factor, which depends on the geometry of the specimen, the Poisson's ratio of the tested material and on details of the load transfer from the jig into the specimen. Please refer to the literature for a detailed description of the apparatus and the thorough theoretical treatment.[26–28] A numerical analysis of the system based on a finite element (FE) simulation has been carried out (*cf.* Fig. 1(b)) in order to calibrate the factor f for this configuration, resulting in values of $f = 1.60$ and $f = 2.07$ for the 2 mm × 2 mm and 3 mm × 4 mm geometries, respectively, for a Poisson's ratio of 0.3.[32]

All B3B tests were carried out in a universal testing machine (Zwick Z010, Zwick/Roell, Ulm, Germany) with the aid of a jig especially designed at ISFK (Leoben, Austria) for very small specimens. Examination of fracture surfaces was carried out with an Olympus BX50 light microscope, an Olympus SZH10 stereo microscope (Olympus, Tokyo, Japan), and with SEM.

3. Results and discussion

3.1. Characterisation of the 3Y-TZP ink

The particle size distribution of the attrition milled suspension was determined and the d_{10}, d_{50}, and d_{90} values (100 nm, 280 nm, and 890 nm, respectively) were measured. The values of the particle size are in agreement with the ones reported in similar studies.[8,13,15] Additionally, no clogging due to large agglomerates was observed in any of the nozzles. The viscosity of the ceramic ink was determined to be ~15 mPa s, which was relatively high compared to the values obtained in previous studies.[16,17] The difference can be explained by the 3 vol.% increase in the solids content of the ink. The surface tension of the ink was measured to be ~42 mN m^{-1}, whereas its density was 2.35 g cm^{-3}.

In order to analyse the printing reliability and the drop characteristics, a single drop array was investigated by SEM. Fig. 2 shows a SEM micrograph of three horizontal rows of drops.
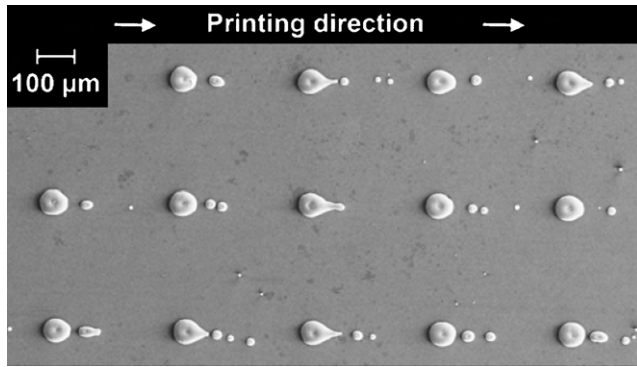
Fig. 2. SEM micrograph of a single drop array printed on a glass substrate.

Fig. 3. Sintered inkjet printed samples with dimensions 2 mm × 2 mm × 0.3 mm (above) and 3 mm × 4 mm × 0.3 mm (below).

Fig. 4. SEM micrograph of the top surface of a sintered 3 mm × 4 mm sample.

Each row was printed by one specific nozzle and not all of the nozzles were active. A nozzle spacing of ∼42 µm and a distance of ∼340 µm between the adjacent rows shows that every eighth nozzle was printing.[33] The similarity in size, shape, and spacing of the drops demonstrates the reliability of the printing process, which can eject and position identical ceramic building units. Secondary droplets can be seen on the right side of the main drops. The presence of such droplets can be explained either by (i) the formation of satellite drops or by (ii) drop splashing upon impact. Case (i) is dominated by the Oh^{-1} number, which defines the limit of the printability region ($1 < Oh^{-1} < 10$). Printing inks with high Oh^{-1} values leads to the formation of an elongated ink column before the drop is detached, thus resulting in the formation of satellite drops. In the case of a small Oh^{-1} number, the viscous forces are dominant and a higher pressure is needed to eject the drop, preventing satellite drop formation.[6,16,31,34] However, it has to be considered that the aforementioned printability region was defined for piezoelectric inkjet printers, where the ejection pressure is considerably low compared to thermal inkjet printers.[35,36] In our case the Oh^{-1} number of the ink was ∼2.5, but since a thermal inkjet printer was used, the production of satellite drops cannot be excluded even if a low Oh^{-1} was obtained.

Regarding case (ii), splashing would occur for Weber numbers (We) > 50.[37,38] This number is a dimensionless fluid constant given by

$$We = \frac{\rho \cdot u^2 \cdot a}{\sigma}, \qquad (4)$$

where u is the drop velocity, which was estimated to be ∼3.4 m s^{-1} assuming a constant ejection pressure for any ink.[17,36] A We number of ∼10 was calculated for the given properties. For such a value splashing should not occur and it can thus be concluded that the smaller drops observed in Fig. 2 have to be ascribed to the formation of satellite drops during drop ejection. This result confirms that the above-defined Oh^{-1} interval can be only a rough estimate of the printability range for thermal inkjet printers. In other words, drop integrity and satellite drop formation cannot be explained solely by the Oh^{-1} number.
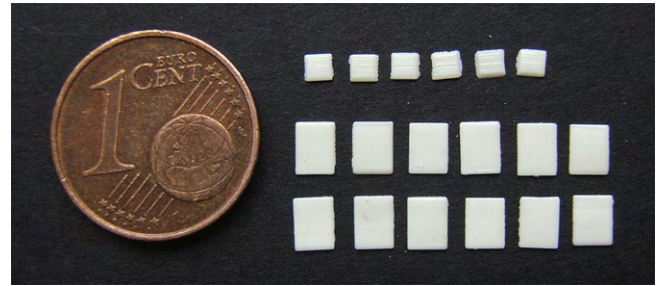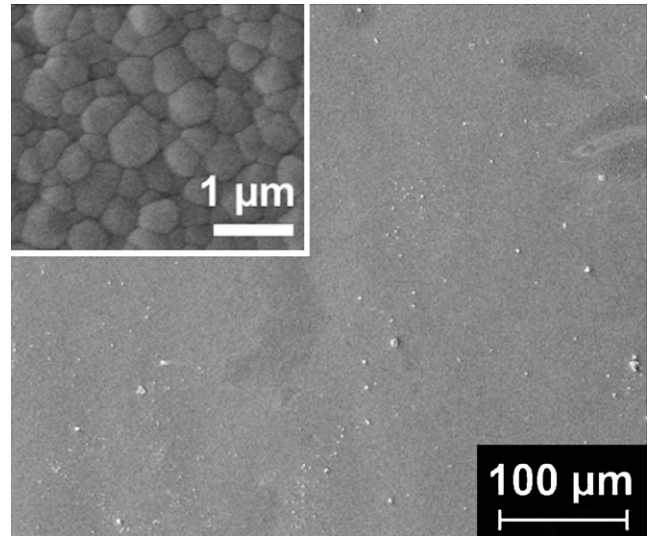
3.2. Evaluation of the sintered specimens

The inkjet printed specimens after sintering resulted in final dimensions of 2 mm × 2 mm × 0.3 mm and 3 mm × 4 mm × 0.3 mm. This corresponds to a linear sintering shrinkage of ∼15%. Fig. 3 shows 6 and 12 pieces of the 2 mm × 2 mm and 3 mm × 4 mm specimens, respectively. Here, the top surfaces of the specimens, which were set under tension during the B3B-test, are visible. It can be inferred from Fig. 3 that all specimens possess a plane parallel structure, which facilitates mechanical testing. This is a consequence of the removal of the specimens from the substrate prior to sintering. A detail of the surface quality can be appreciated in Fig. 4 for a 3 mm × 4 mm specimen. The specimen surface is smooth and shows no large process-related defects, such as unprinted regions, textured structures due to drop reliefs, or scratches parallel to the printing direction. On the left corner of Fig. 4, a detailed SEM micrograph shows the microstructure, revealing an average grain size below 1 µm.

3.3. Strength tests results and fractography

Fig. 5 shows the results of B3B tests conducted both on the inkjet printed 3Y-TZP specimens (*i.e.* 2 mm × 2 mm and 3 mm × 4 mm) and on the hot-pressed 3Y-TZP (for comparison).
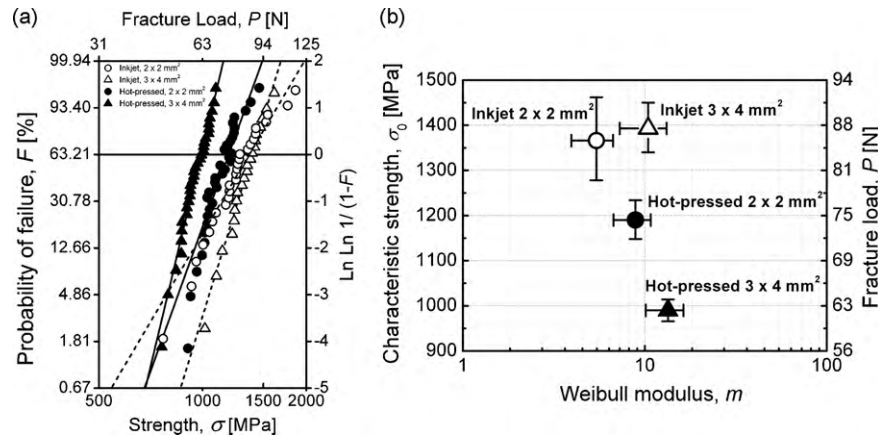
Fig. 5. (a) Failure strength vs. probability of failure diagram showing the strength distribution to fracture of inkjet printed and hot-pressed samples of both geometries. (b) Weibull modulus vs. nominal characteristic strength diagram comparing the results of the statistical analyses.

The failure stress vs. the probability of failure of the tested specimens is presented in Fig. 5(a) in a Weibull diagram. The scale chosen in the graph allows representing Weibull-distributed data as a straight line. Each distribution was collected on a sample of 30 specimens, which ensures statistical significance for the Weibull analysis.[20–22] Fig. 5(b) reports the Weibull moduli, m (biased) vs. the nominal characteristic strength σ_0 (*i.e.* the stress with a probability of failure of $F = 63.21\%$), for all four specimen sets. All data are listed in Table 1 including the 90% confidence interval. Following the principle of independent actions (PIA), the effective volume, V_{eff}, for the two geometries has been calculated with the FE analysis for the corresponding m, and is also reported in Table 1.

Based on a linear elastic fracture mechanics (LEFM) approach, the critical defect size (a_c) causing the failure can be estimated based on the failure stress, σ_f, and fracture toughness, K_{Ic}, of the material as given by the following equation[21]:

$$a_c = \frac{1}{\pi}\left(\frac{K_{Ic}}{Y \cdot \sigma_f}\right)^2, \qquad (5)$$

where Y is a dimensionless geometric factor depending on the shape of the defect and loading configuration. Assuming a characteristic fracture toughness value for 3Y-TZP of 5 MPa m$^{1/2}$,[39] and a geometric factor of $Y = 2/\pi$ (corresponding to small cracks or embedded circular flaws at the surface), a critical flaw size distribution has been estimated for each sample (see Table 1). The upper and lower values of the given defect range correspond to the lowest and highest failure stress from each tested sample.

By comparing the strength values of inkjet specimens and hot-pressed specimens (Fig. 5), a better mechanical performance of the former can be observed, independent of the geometry tested, resulting in $\sigma_0 = 1366$ (vs. 1190) MPa for the 2 mm × 2 mm specimens and $\sigma_0 = 1393$ (vs. 990) MPa for the 3 mm × 4 mm ones. In terms of Weibull modulus, m, all sets range within the same values (*i.e.* between 7 and 16), besides the inkjet printed 2 mm × 2 mm specimens which show a relatively low m (*i.e.* between 4 and 7). This suggests a wider critical flaw size distribution in this set (see Table 1), as estimated by Eq. (5).

In order to clarify the origin of failure in all these sets, a fractographic analysis has been performed on some of the broken specimens.

Figs. 6 and 7 show SEM micrographs of the fracture surfaces of tested specimens with both 2 mm × 2 mm and 3 mm × 4 mm geometries. Although these specimens consisted of 65 deposited layers, no trace of delamination in the structure could be discerned. This indicates that the drying conditions were suitable for the single layers to merge together instead of forming laminates due to drying stresses. The microstructure of the specimens in Figs. 6 and 7 reveals no process-related defects and a very low porosity, which indicates that uniform microstructure as well as a full density was achieved after sintering.

The fracture surfaces in Figs. 6(a) and 7(a) belong to specimens that fractured at low applied stress values and reveal a clear symmetry with presence of fracture mirror. Specimens with higher strength underwent significant fragmentation due to the release of the stored elastic energy, which complicated *post-mortem* (fractographic) examinations. Critical defects were

Table 1

Characteristic strength and Weibull modulus of the two materials for each geometry, with the corresponding calculated effective volume and estimated critical defect size. The 90% confidence intervals are also represented.

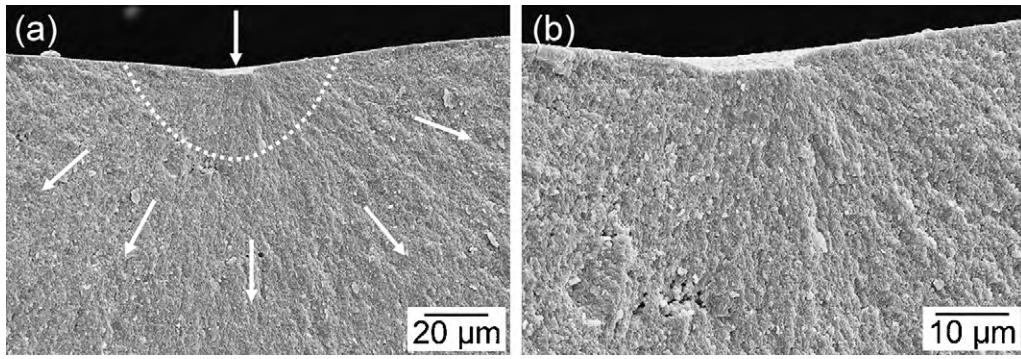| Sample	Characteristic strength, σ_0 [MPa]	Weibull modulus, m	$V_{eff(PIA)}$ [mm³]	a_c [µm] (min–max)
Inkjet printed 2 × 2	1366 [1278–1462]	5.4 [3.9–6.7]	0.00175	(6–33)
Inkjet printed 3 × 4	1393 [1340–1450]	10.4 [7.3–13.2]	0.00049	(8–19)
Hot-pressed 2 × 2	1190 [1148–1234]	8.9 [6.7–10.8]	0.00051	(9–24)
Hot-pressed 3 × 4	990 [966–1014]	13.4 [10.1–16.3]	0.00026	(17–34)

Fig. 6. (a and b) SEM micrographs of the fracture surface of a 2 mm × 2 mm inkjet printed sample after B3B testing. Fracture occurred at the tensile surface (indicated by a downward arrow in (a)) and with a failure stress of $\sigma_f = 1264$ MPa. Hackle lines are also represented by arrows. The dashed line in (a) highlights the fracture mirror. (b) shows at a higher magnification the area containing the critical defect ($a_c = 12.3$ μm), which can be interpreted as an uneven location produced by DIP.
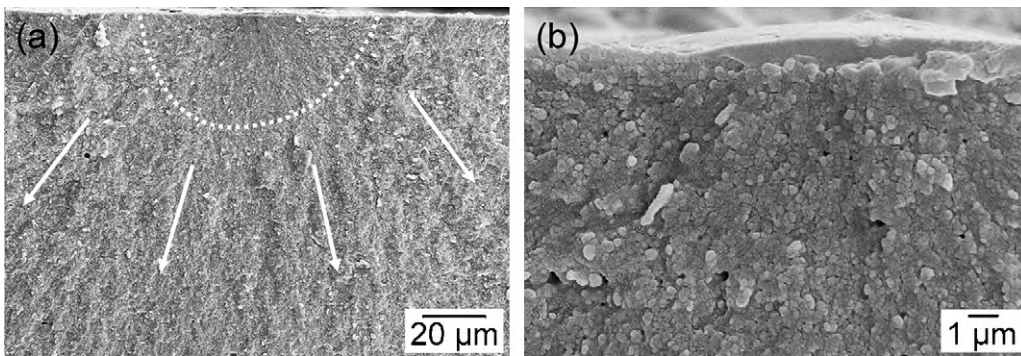

Fig. 7. (a and b) SEM micrographs of the fracture surface of a 3 mm × 4 mm inkjet printed sample after B3B testing. Fracture occurred at the tensile surface and with a failure stress of $\sigma_f = 1348$ MPa. Hackle lines are represented by arrows. The dashed line in (a) highlights the fracture mirror. (b) shows at a higher magnification the critical defect ($a_c = 10.8$ μm), which is also in this case constituted by an uneven location produced by DIP.

found mostly on the top surface (*cf.* Figs. 6 and 7), and could be interpreted as uneven locations due to the surface roughness. As DIP is an additive process using very fine (~35 pl) drops as building units, the top surface of a specimen always comprises a certain level of roughness (although very low for drops of this size). It is thus supposed that, in absence of other microstructural defects or processing damage, even the smallest roughness on the surface subjected to tensile stress during B3B-testing can be critical. The size of the defects observed in Figs. 6 and 7 is indeed in agreement with the critical defect size range estimated with Eq. (5)

by means of fracture mechanics based on the B3B strength results.

Fracture surfaces of 2 mm × 2 mm and 3 mm × 4 mm hot-pressed 3Y-TZP specimens are reported in Figs. 8 and 9, respectively. In comparison to the inkjet printed samples, in the hot-pressed 3Y-TZP a high roughness and poor symmetry is found, which hinders the observation of the fracture mirror. The precise determination of the fracture origin is thus difficult, and can be based only on the location of (coarse) hackle lines.[40,41] The non-localised nature of the fracture origin in Figs. 8 and 9 suggests the presence of a porosity-related extended defect at
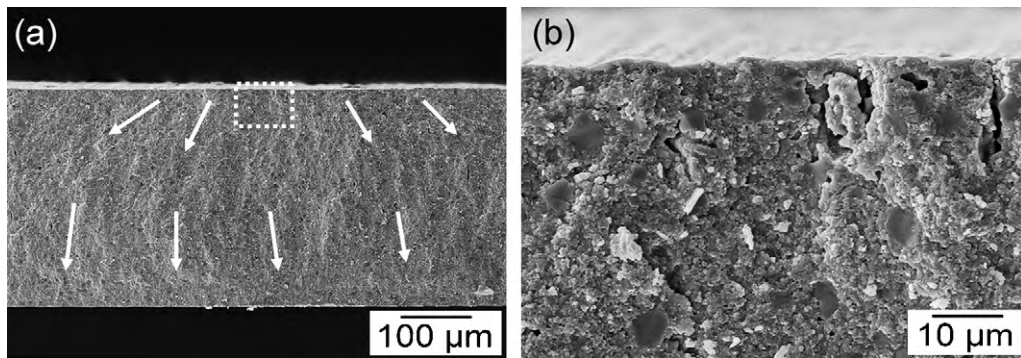

Fig. 8. SEM micrographs of the fracture surface of a 2 mm × 2 mm hot-pressed sample after B3B testing. Fracture occurred at a failure stress of $\sigma_f = 1088$ MPa. Fracture origin is hardly visible due to the absence of a fracture mirror and the presence of coarse hackle lines (a), indicated by arrows. Large pores and agglomerates that could be responsible for fracture are shown in (b) at a higher magnification. The calculated critical defect size for this specimen is $a_c = 16.6$ μm.
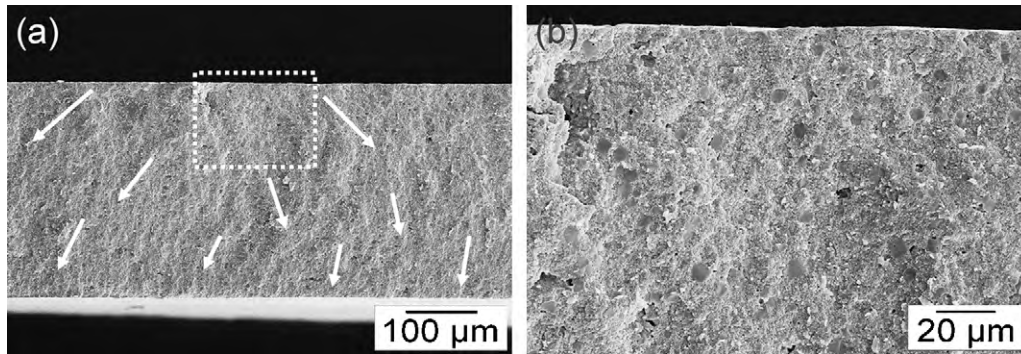
Fig. 9. SEM micrographs of the fracture surface of a 3 mm × 4 mm hot-pressed sample after B3B testing. Fracture occurred at a failure stress of $\sigma_f = 761$ MPa. Fracture origin is hardly visible due to the absence of a fracture mirror and the presence of coarse hackle lines (a), indicated by arrows. The area where fracture most likely originated is shown in (b) with a higher magnification. The calculated critical defect size for this specimen is $a_c = 33.9$ μm.

the starting point. Some of the bigger pores have an elongated shape (*cf.* Fig. 8(b)), which could be ascribed to the production process. In this regard, inkjet printing produces a lower amount of sub-micron pores with a round shape, whereas pores due to hot-pressing have dimensions up to tens of microns and irregular shapes. They are thus in the range of the critical defects for these specimens (see Table 1), and could be responsible for their failure. In the inkjet printed samples the pores dimensions are much smaller than the critical defects, which are thus constituted solely by surface features, as already remarked (*cf.* Figs. 6 and 7).

The hot-pressed 3Y-TZP in Figs. 8 and 9 presents also a consistent amount of a second phase, which could be constituted by cubic 3Y-TZP grains. Although this phase could in principle improve the mechanical properties of the ceramic bulk, the relatively large size of the critical defects (pores and agglomerates) here dramatically lowers the overall strength of the material.

It can thus be concluded that the difference in characteristic strength between the inkjet printed and the hot-pressed 3Y-TZP samples has to be ascribed to the difference in the size and nature of the critical defects originated by the respective production processes. In the inkjet printed specimens failure starts always from small imperfections at the tensile surface, which are likely due to traces/reliefs of building drops during printing. On the other hand, large pores and agglomerates are responsible for the early fracture of the hot-pressed 3Y-TZP. In other words, the lower porosity obtained with the DIP process significantly increased the strength of the 3Y-TZP material.

4. Summary and conclusions

Miniaturised 3Y-TZP specimens of different dimensions (*i.e.* 2 mm × 2 mm and 3 mm × 4 mm) were produced by direct inkjet printing (DIP) using a thermal inkjet printer and mechanically tested under biaxial loading. The aqueous ink was prepared and characterised in terms of particle size distribution, viscosity, surface tension, and *Oh* number. The fracture biaxial strength of the printed specimens was evaluated using the ball-on-three-balls test. A fractographic analysis was performed to identify the source of failure. Results were compared to hot-pressed 3Y-TZP specimens taken as reference material.

It was found that the inkjet printed samples possessed a higher strength compared to the reference material, which can be ascribed to the better microstructure obtained using the DIP process. In particular, DIP allowed full density to be achieved, and the absence of volume defects improved the mechanical strength of these specimens. Fracture in inkjet printed samples originated always at small imperfections at the tensile surface, whereas hot-pressed samples failed due to large pores or agglomerates. As a result, it can be concluded that the DIP process is suitable for the production of defect-free, high-strength ceramic components for microelectronic applications. Moreover, DIP can be classified as a rapid manufacturing technology and it can be employed to produce structural ceramic components of relatively small dimensions.

Acknowledgements

References

1. Blazdell PF, Evans JRG, Edirisinghe MJ, Shaw P, Binstead MJ. The computer aided manufacture of ceramics using multilayer jet printing. *J Mater Sci Lett* 1995;**14**:1562–5.
2. Slade CE, Evans JRG. Freeforming ceramics using a thermal jet printer. *J Mater Sci Lett* 1998;**17**:1669–71.
3. Mott M, Evans JRG. Zirconia/alumina functionally graded material made by ceramic ink jet printing. *Mater Sci Eng* 1999;**271**(A):344–52.
4. Mott M, Song JH, Evans JRG. Microengineering of ceramics by direct ink-jet printing. *J Am Ceram Soc* 1999;**82**(7):1653–8.

5. Windle J, Derby B. Ink jet printing of PZT aqueous ceramic suspensions. *J Mater Sci Lett* 1999;**18**:87–90.

6. Seerden KAM, Reis N, Evans JRG, Grant PS, Halloran JW, Derby B. Ink-jet printing of wax-based alumina suspensions. *J Am Ceram Soc* 2001;**84**(11):2514–20.

7. Ainsley C, Reis N, Derby B. Freeform fabrication by controlled droplet deposition of powder filled melts. *J Mater Sci Lett* 2002;**37**:3155–61.

8. Derby B, Reis N. Inkjet printing of highly loaded particulate suspensions. *MRS Bull* 2003;**28**:815–8.

9. Lee DH, Derby B. Preparation of PZT suspensions for direct ink jet printing. *J Eur Ceram Soc* 2004;**24**:1069–72.

10. Zhao X, Evans JRG, Edirisinghe MJ, Song JH. Ink-jet printing of ceramic pillar arrays. *J Mater Sci* 2002;**37**:1987–92.

11. Zhao X, Evans JRG, Edirisinghe MJ, Song JH. Direct ink-jet printing of vertical walls. *J Am Ceram Soc* 2002;**85**(8):2113–5.

12. Song JH, Nur HM. Defects and prevention in ceramic components fabricated by inkjet printing. *J Mater Proc Technol* 2004;**155**(6):1286–92.

13. Cappi B, Özkol E, Ebert J, Telle R. Direct inkjet printing of Si_3N_4: characterization of ink, green bodies and microstructure. *J Eur Ceram Soc* 2008;**28**(13):2625–8.

14. Ebert J, Özkol E, Zeichner A, Uibel K, Weiss Ö, Koops U, et al. Direct inkjet printing of dental prostheses made of zirconia. *J Dent Res* 2009;**88**(7):673–6.

15. Lejeune M, Chartier T, Dossou-Yovo C, Noguera R. Ink-jet printing of ceramic micro pillar arrays. *J Eur Ceram Soc* 2009;**29**:905–11.

16. Özkol E, Ebert J, Uibel K, Wätjen AM, Telle R. Development of high solid content aqueous 3Y-TZP suspensions for direct inkjet printing using a thermal inkjet printer. *J Eur Ceram Soc* 2009;**29**(3):403–9.

17. Özkol E, Ebert J, Telle R. An experimental analysis of the influence of the ink properties on the drop formation for direct thermal inkjet printing of high solid content aqueous 3Y-TZP suspensions. *J Eur Ceram Soc* 2010;**30**(7):1669–78.

18. Coombs Jr CF. *Printed circuits handbook*. 6th ed. New York: McGraw-Hill; 2008, 21.1.

19. Jillek W, Jung WKC. Embedded components in printed circuit boards: a processing technology review. *Int J Adv Manuf Technol* 2005;**25**:350–60.

20. Weibull W. A statistical distribution function of wide applicability. *J Appl Mech* 1951;**18**:293.

21. Danzer R, Lube T, Supancic P, Damani R. Fracture of ceramics. *Adv Eng Mater* 2008;**10**(4):275–96.

22. Danzer R. Some notes on the correlation between fracture and defect statistics: are Weibull statistics valid for very small specimens? *J Eur Ceram Soc* 2006;**26**:3043–9.

23. Börger A, Supancic P, Danzer R. The ball on three balls test for strength testing of brittle discs: stress distribution in the disc. *J Eur Ceram Soc* 2002;**22**:1425–36.

24. Börger A, Supancic P, Danzer R. The ball on three balls test for strength testing of brittle discs. Part II. Analysis of possible errors in the strength determination. *J Eur Ceram Soc* 2004;**24**:2917–28.

25. Danzer R, Supancic P, Harrer W. Biaxial tensile strength test for brittle rectangular plates. *J Ceram Soc Jpn* 2006;**114**(11):1054–60.

26. Danzer R, Harrer W, Supancic P, Lube T, Wang Z, Börger A. The ball on three balls test—strength and failure analysis of different materials. *J Eur Ceram Soc* 2007;**27**(2–3):1481–5.

27. Morrell R, McCormick NJ, Bevan J, Lodeiro M, Margetson J. Biaxial disc flexure—modulus and strength testing. *Br Ceram Trans* 1999;**98**:234–40.

28. Godfrey DJ, John S, Disc flexure tests for the evaluation of ceramic strength In: Lübeck-Travemünde, editor. *Ceramic materials and components for engines*. 1986. p. 657–65.

29. Lee ER. *Microdrop generation*. Florida: CRC Press; 2002 [Chapter 13].

30. Kang HR. Water-based ink-jet ink. I. Formulation. *J Imaging Sci* 1991;**35**:179–88.

31. Lewis JA, Smay JE, Stuecker J, Cesarano III J. Direct ink writing of three-dimensional ceramic structures. *J Am Ceram Soc* 2006;**89**(12):3599–609.

32. Ceramics: single oxides. In: *ASM engineered materials reference book* (2nd ed.). Bauccio, ML: The Materials Information Society; 1994. p. 252–64.

33. Shelley DJ, Majewski JT, Thackray MR, McWilliams JL. A lower-cost inkjet printer based on a new printing performance architecture. *Hewlett-Packard J* 1997;**48**(3):6–11.

34. Jang D, Kim D, Moon J. Influence of fluid physical properties on ink-jet printability. *Langmuir* 2009;**25**:2629–35.

35. Rembe C, aus der Wiesche S, Hofer EP. Thermal ink jet dynamics: modelling, simulation, and testing. *Microelectron Reliab* 2000;**40**(3):525–32.

36. Wijshoff HMA. *Structure- and fluid-dynamics in piezo inkjet printheads*. PhD Thesis, University of Twente, Enschede/The Netherlands; 2008.

37. Ren M, Wijshoff H. Thermal effect on the penetration of an ink droplet onto a porous medium. In: Stoffels GGM, van der Meer TH, van Steenhoven AA, editors. *Proceedings 5th European thermal-sciences conference*. ISBN 978-90-386-1274-4; 2008.

38. Clarke A, Blake TD, Carruthers K, Woodward A. Spreading and imbibition of liquid droplets on porous surfaces. *Langmuir* 2002;**18**:2980–4.

39. Ashby MF. *Materials selection in mechanical design*. 3rd ed. München/Germany: Elsevier; 2007.

40. Morrell R. *Fractography of brittle materials. Measurement good practice guide no. 14*. ISSN 1368-6550. Teddington/UK: National Physical Laboratory; 1999.

41. Quinn GD. *Fractography of ceramics and glasses*. Washington: National Institute of Standards and Technology, Spec. Publ. 960-17; 2006.